IEEE Access
Multidisciplinary | Rapid Review | Open Access Journal

Received August 26, 2019, accepted September 16, 2019, date of publication September 23, 2019, date of current version October 8, 2019.

Digital Object Identifier 10.1109/ACCESS.2019.2943111

Establishment of a Wideband Radar Scattering Center Model of a Plasma Sheath

XI ZHANG[1], YANMING LIU[1], BOWEN BAI[1], XIAOPING LI[1], FANGFANG SHEN[1], XU-YANG CHEN[1], AND LIANG ZHAO[2]

[1]School of Aerospace Science and Technology, Xidian University, Xi'an 710026, China
[2]Science and Technology on Space Physics Laboratory, Beijing 100076, China

Corresponding author: Bowen Bai (bwbai@xidian.edu.cn)

This work was supported in part by the National Natural Science Foundation of China under Grant 61701381, Grant 61431010, and Grant 61627901, in part by the Chinese Postdoctoral Science Foundation, and in part by the Natural Science Basic Research Plan in Shaanxi Province of China under Grant 2019JM-177.

ABSTRACT A reentry object covered by a plasma sheath will produce two reflective signals in a radar echo, which seriously affects the detection of the reentry object by radar and results in positioning error and even tracking loss. On the basis of the scattering center model and the non-uniform plasma stratification model, the present paper establishes a radar scattering model of a reentry object covered by a plasma sheath. The model effectively retains the plasma distribution and electromagnetic wave propagation characteristics of the plasma sheath. Analysis of the signal components of radar echoes in an example shows to some extent that the non-mirror reflection signal is not generated by the plasma wake.

INDEX TERMS Plasma sheath, scattering centers, Doppler effect, wideband radar, transmission line analogy.

I. INTRODUCTION

In the reentry flight environment, plasma generated by the aerothermal effect forms a sheath, which contains a large number of free electrons and has strong reflection, refraction, absorption, and attenuation effects on electromagnetic waves [1]. On the one hand, the plasma sheath will electromagnetically interfere with the radar signal, which will affect the accuracy and accuracy of radar detection; on the other hand, it will produce two reflection signals [2]–[5] in the radar echo, which will affect target detection and recognition and even cause a tracking loss, as shown in Figure 1. To minimize or remove the adverse effects of the plasma sheath on radar detection, it is highly desirable to explore the mechanism of the effect of the plasma sheath on radar detection and improve the method of processing the target radar signal.

Research on signal processing of the plasma sheath began in the 1960s, aiming at solving the problem of ''black-barrier'' communication and mainly focusing on the propagation characteristics of electromagnetic waves in plasma [6]–[10]. Until the last decade, research on radar detection under the influence of the plasma sheath has been open one after another, mainly focusing on the effect of the attenuation of the electromagnetic signal on the target radar cross section (RCS) [11]–[14]. In addition, X. Y. Chen et al. simulated inhomogeneous plasma with multi-layer media and studied the amplitude attenuation and phase change of the radar echo signal with vertical incidence under the effect of the plasma

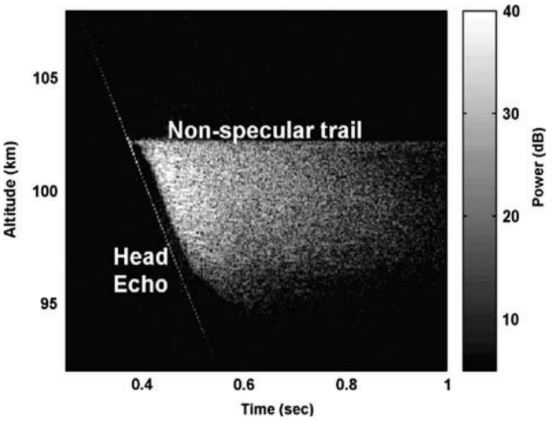

FIGURE 1. Altitude–time–intensity image of a head and subsequent non-specular echoes over an extended range from ALTAIR VHF radar. The diagonal line to the left is called the head echo, while the echoes spreading in range and time to the right are the non-specular trail. Figure reproduced from Close et al.

The associate editor coordinating the review of this manuscript and approving it for publication was Nagendra Prasad Pathak.

sheath [15]. Besides the amplitude attenuation and phase change of the target radar echo signal, the plasma sheath itself reflects and generates a radar echo signal [16]–[18]. There are thus two electromagnetic reflection signals in the radar echo, which has been confirmed in meteor plasma radar detection, as shown in Figure 1 [2], [3]. Based on the unique electromagnetic interference phenomenon of plasma sheath, in recent years, the research on the causes of this phenomenon has been gradually carried out, and the new technology of radar jamming using plasma has been developed [19], [20].

At present, the two reflected signals produced by meteor plasma are mostly considered to correspond to the high-concentration plasma enclosing the meteor body and the wake generated during the dissipation of the plasma, but there is no decisive conclusion. The radar detection of meteor plasma also focuses on the RCS calculation of the head echo.

Referring to the radar detection results of meteor plasma, the reentry object should also have two reflection signals under the influence of the plasma sheath. To explore the causes of the two reflected signals, it is not enough to focus only on the RCS of the target in the static state, but rather to consider also the radar echo characteristics of the plasma sheath. The present paper calculates the reflection intensity distribution of the reentry plasma sheath and investigates the Doppler characteristics of the radar echo. The paper therefore establishes a radar scattering model that satisfies the hypersonic flow field distribution of the plasma sheath. The radar echo data are obtained by simulation, and the causes of a non-specular trail are preliminarily analyzed.

The paper is organized as follows. Section II introduces the principles used in our model. Section III describes the establishment of the model and the generation of radar echoes. Section IV takes a blunt cone as an example with which to simulate and analyze the signal components of the target reflection signal. Section V presents conclusions and further discussions.

II. PRINCIPLE

A. SCATTERING CENTER MODEL

According to the geometric theory of diffraction (GTD) [10], the radar wavelength is much smaller than the target size when a radar system operates in the optical region. The target echo can be considered the superposition of strong electromagnetic scattering at the local position of the target. These localized electromagnetic scattering sources are called equivalent scattering centers [21], [22]. The radar target echo E is defined as

$$\mathrm{E}(\varphi, \gamma, f_R) = \sum_{m=1}^{M} \Gamma_m e^{-j4\pi f_R r_m(\varphi,\gamma)/c}, \tag{1}$$

where f_R is the reflection frequency, φ is the azimuth angle, γ is the elevation angle, M is the number of target scattering centers, Γ_m is the complex amplitude corresponding to the mth scattering (i.e., the complex scattering coefficient), (x_m, y_m, z_m) is the spatial location corresponding to the mth scattering center, and c is the speed of light. In addition, the one-dimensional projection position of each scattering center in the radar line of sight is expressed by

$$r_m(\varphi, \gamma) = x_m \cdot \cos\gamma \cos\varphi + y_m \cdot \cos\gamma \sin\varphi + z_m \cdot \sin\gamma. \tag{2}$$

Formulas (1) and (2) show that the target echo can be simulated when the scattering center and radar parameters are known.

B. LAYERED MODEL FOR A NON-UNIFORM PLASMA SHEATH

The reentry plasma sheath is a non-uniform and non-magnetized plasma fluid and can be characterized by the electron density and collision frequency as parameters. The layered model used to simulate the plasma sheath is approximately constructed from uniform plasma plates with different thickness according to the profile of the electron density distribution, as shown in Fig. 2.

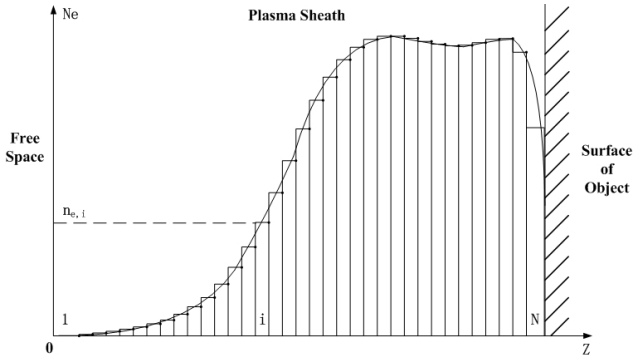

FIGURE 2. Layered model for simulating the reentry plasma sheath. The left side is free space for electromagnetic wave incidence and the right side is the surface of the reentry object.

Along the vertical direction of the reentry object surface, the plasma electron density approximately follows a bi-Gaussian distribution. On this basis, the plasma sheath is divided into N-layer uniform plasma slabs. For the homogeneous plasma in the ith layer, the plasma frequency $\omega_{p,i}$ is [8]

$$\omega_{p,i} = \sqrt{\frac{n_{e,i}e^2}{m_e\varepsilon_0}}, \tag{3}$$

where $n_{e,i}$ is the electron density of the ith layer (m^{-3}), e is the unit charge (C), m_e is the electron mass (kg), and ε_0 is the vacuum dielectric constant.

In the ith layer, the complex dielectric coefficient $\tilde{\varepsilon}_i$ is

$$\tilde{\varepsilon}_i = \left[1 - \frac{\omega_{p,i}^2}{\omega^2 + v_i^2} - j \cdot \frac{v_i}{\omega} \cdot \frac{\omega_{p,i}^2}{\omega^2 + v_i^2}\right] \cdot \varepsilon_0 \tag{4}$$

and the wave vector is

$$k_i = \omega\sqrt{\mu_0\tilde{\varepsilon}_i}, \tag{5}$$

where v_i is the collision frequency, ω is the frequency of the incident wave (rad/s), and μ_0 is the permeability of vacuum. The permeability of air and plasma is equal to that of vacuum.

C. ANALOGY OF A TRANSMISSION LINE

A standing wave pattern forms along the z-axis owing to multiple internal reflections in the multilayer structure. The multilayer structure along the z-axis is thus equivalent to the cascade of transmission lines with different effective impedance of each medium. In this case, the analogy of the transmission line [23]–[25] is applied to determine the reflection coefficient of the layered model.

The angle of refraction/reflection θ_i can be obtained using Snell's law, $k_0 \sin\theta_0 = k_1 \sin\theta_1 = \cdots k_i \sin\theta_i \cdots = k_N \sin\theta_N$, where θ_0 and k_0 are respectively the incident angle and wave vector in free space.

The transmission matrix of the ith layer is

$$\begin{bmatrix} A_i & B_i \\ C_i & D_i \end{bmatrix} = \begin{bmatrix} \cosh\left(j\tilde{k}_{iz}d_i\right) & Z_i \sinh\left(j\tilde{k}_{iz}d_i\right) \\ \sinh\left(j\tilde{k}_{iz}d_i\right)/Z_i & \cosh\left(j\tilde{k}_{iz}d_i\right) \end{bmatrix}, \quad (6)$$

where

$$Z_i = \begin{cases} \sqrt{\mu_0/\tilde{\varepsilon}_i}\sec\theta_i & \textit{for perpendicular polarization} \\ \sqrt{\mu_0/\tilde{\varepsilon}_i}\cos\theta_i & \textit{for parallel polarization}. \end{cases} \quad (7)$$

The transmission matrix of the N-layered layered model is therefore the cascade of the transmission matrix of each layer:

$$\begin{bmatrix} A & B \\ C & D \end{bmatrix} = \begin{bmatrix} A_1 & B_1 \\ C_1 & D_1 \end{bmatrix} \begin{bmatrix} A_2 & B_2 \\ C_2 & D_2 \end{bmatrix} \cdots \begin{bmatrix} A_N & B_N \\ C_N & D_N \end{bmatrix}. \quad (8)$$

The conventional reflection coefficients of the layered model are then determined using network theory as [11]

$$R = \frac{(A + B/Z_{N+1}) - Z_0(C + D/Z_{N+1})}{(A + B/Z_{N+1}) + Z_0(C + D/Z_{N+1})}, \quad (9)$$

where Z_0 is the characteristic impedance in the incident medium and Z_{N+1} is the characteristic impedance in the reflection medium.

In the present study, the incident medium is air while the reflection medium is determined by the incident depth of the electromagnetic wave (i.e., the number of plasma slabs penetrated). When the electromagnetic wave is reflected at the layered interface of the inhomogeneous plasma, the reflection medium is plasma and the reflection coefficient is calculated using formula (8). When the electromagnetic wave reflects from the surface of the reentry object, the reflection medium is metal. At this time, $Z_{N+1} = 0$ and the reflection coefficient is calculated as

$$R = \frac{B - Z_0 \cdot D}{B + Z_0 \cdot D}. \quad (10)$$

III. MODELING

The shape of the plasma sheath is affected by the structure of the reentry object and flight speed and is that of a fluid. As a whole, the reentry object covered by the plasma sheath constitutes a fluid-covered rigid body. Whether the plasma is penetrated by an electromagnetic wave depends on both the plasma frequency and electromagnetic wave frequency. The scattering model must conform to this structure to reflect the semi-permeability of plasma to an electromagnetic wave.

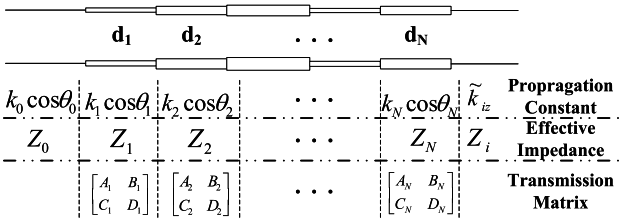

FIGURE 3. Analogy of the transmission line of the layered model. The N-layered model is equivalent to the cascade of transmission lines with different impedance. For the ith equivalent transmission line, the length is denoted d_i, the equivalent propagation constant along the z-axis is denoted $\tilde{k}_{iz}$, and Z_i is the characteristic impedance in the layer.

Taking a blunt cone as an example, a model of the scattering center of the reentry object covered by a plasma sheath is established.

The parameters of the layered model are the electron density n_e, collision frequency v, thickness d, airflow velocity V_f, and total number of layers N. The direction of the airflow velocity V_f is toward the scattering center by the stationary point, parallel to the surface of the blunt cone.

The incident depth of the electromagnetic wave is different for each scattering center. The plasma frequency is also called the cut-off frequency. When $\omega < \omega_p$, the electromagnetic wave cannot penetrate. The reflection of the electromagnetic wave therefore occurs only at the interface of the plasma slab outside the red curve and is strongest at the red curve. If the electromagnetic wave can penetrate the plasma, the reflection of the electromagnetic wave is strongest on the surface of the reentry object. To reduce the computational complexity, the present paper only considers the strongest component of the electromagnetic wave reflected by the scattering centers.

The steps are described by the flow chart in Fig. 5. The details are as follows:

Step 1: According to the structure of the target, the target is divided into M scattering centers, and the spatial position of the mth scattering centers is (x_m, y_m, z_m), $m = 1, 2, \cdots, M$;

Step 2: For the mth scattering center, the corresponding layered model includes the following parameters:

Electron density $n_{e,mi}$, collision frequency v_{mi}, thickness d_{mi}, airflow velocity $V_{f,mi}$, total number of layers N_m,where $i = 1, 2, \cdots, N_m$. The farthest plasma plate from the reentry object surface is the first layer.

At the same time, according to equation (3,4,5), the plasma frequency, plasma relative permittivity and wave vector can be obtained as follows:

$$\omega_{p,mi} = \sqrt{\frac{n_{e,mi}e^2}{m_e\varepsilon_0}}, \quad (11)$$

$$\tilde{\varepsilon}_{mi} = \left[1 - \frac{\omega_{p,mi}^2}{\omega^2 + v_{mi}^2} - j \cdot \frac{v_{mi}}{\omega} \cdot \frac{\omega_{p,mi}^2}{\omega^2 + v_{mi}^2}\right] \cdot \varepsilon_0, \quad (12)$$

$$k_{mi} = \omega\sqrt{u_0\tilde{\varepsilon}_{mi}}. \quad (13)$$

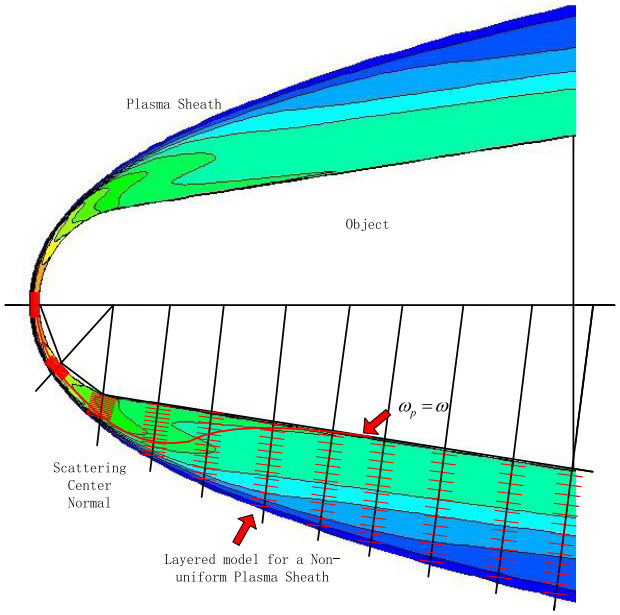

FIGURE 4. Model of the scattering center of a reentry object covered by a plasma sheath. A number of scattering centers are taken on the surface of the reentry object. The normal of each scattering center is perpendicular to the surface of the object. On the basis of the surface of the object, parallel layers are established at each scattering center. The layers are independent of each other. The red curve in the plasma sheath represents the position where the plasma frequency ω_p is equal to the electromagnetic wave frequency ω.

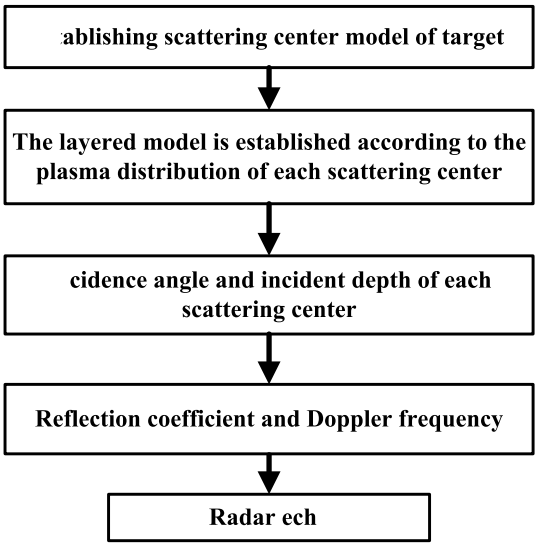

FIGURE 5. Flow chart of radar echo generation for scattering centers.

Step 3: The centrosymmetric axis of the target is parallel to the Y axis. For the mth scattering center, the angle between the electromagnetic wave and the normal line of the target surface, that is, the incident angle of the electromagnetic wave is:

$$\theta_m = \arctan\sqrt{\tan^2\theta_{mxy} + \tan^2\theta_{myz}}, \tag{14}$$

where θ_{mxy} and θ_{myz} are projections of incident angle θ_m on the XY plane and YZ plane respectively, and they satisfy the following relation:

$$\theta_{mxy} = \theta_{mnxy} + \varphi, \tag{15}$$

$$\theta_{myz} = \theta_{mnyz} - \gamma, \tag{16}$$

where θ_{mnxy} and θ_{mnyz} are the angles between the projection of the normal line on the XY plane and the YZ plane and the Y axis, respectively.

For the mth scattering center, the plasma frequency $\omega_{p,mi}$ and electromagnetic wave frequency ω are compared layer by layer from first layer. When $\omega_{p,mi} \geq \omega$, the electromagnetic wave cannot penetrate the ith layer plasma plate, and the incident depth L_m is as follows:

$$L_m = i - 1. \tag{17}$$

If the electromagnetic wave frequency ω is greater than the plasma frequency $\omega_{p,mi}$ of all plasma plates, the incident depth L_m is as follows:

$$L_m = N_m. \tag{18}$$

Step 4: For the ith layer plasma plate of the mth scattering center, the propagation constant is expressed by

$$\tilde{k}_{miz} = k_{mi}\cos\theta_{mi}, \tag{19}$$

where, $\cos\theta_{mi} = \sqrt{1 - \left(\sqrt{\frac{\varepsilon_0}{\tilde{\varepsilon}_{mi}}}\sin\theta_m\right)^2}$. Based on (6) and (19), the transmission matrix is

$$\begin{bmatrix} A_{mi} & B_{mi} \\ C_{mi} & D_{mi} \end{bmatrix} = \begin{bmatrix} \cosh(j\tilde{k}_{miz}d_{mi}) & Z_{mi}\sinh(j\tilde{k}_{miz}d_{mi}) \\ \sinh(j\tilde{k}_{miz}d_{mi})/Z_{mi} & \cosh(j\tilde{k}_{miz}d_{mi}) \end{bmatrix}, \tag{20}$$

where

$$Z_{mi} = \begin{cases} \sqrt{\mu_0/\tilde{\varepsilon}_{mi}}\sec\theta_{mi} & \textit{for perpendicular polarization} \\ \sqrt{\mu_0/\tilde{\varepsilon}_{mi}}\cos\theta_{mi} & \textit{for parallel polarization.} \end{cases} \tag{21}$$

And, the transmission matrix of the mth scattering center as shown in the following:

$$\begin{bmatrix} A & B \\ C & D \end{bmatrix} = \begin{bmatrix} A_{m1} & B_{m1} \\ C_{m1} & D_{m1} \end{bmatrix}\begin{bmatrix} A_{m2} & B_{m2} \\ C_{m2} & D_{m2} \end{bmatrix}\cdots\begin{bmatrix} A_{mL_m} & B_{mL_m} \\ C_{mL_m} & D_{mL_m} \end{bmatrix}. \tag{22}$$

At this time, the reflection coefficient can be expressed by (23), as shown at the top of the next page, where the effective impedances of the parallel polarized wave are $Z_{m0} = \sqrt{u_0/\varepsilon_0}\cos\theta_m$, $Z_{mL_m+1} = \sqrt{u_0/\varepsilon_{mL_m+1}}\cos\theta_{mL_m+1}$, $\cos\theta_{mL_m+1} = \sqrt{1 - \left(\sqrt{\frac{\varepsilon_0}{\varepsilon_{mL_m+1}}}\sin\theta_m\right)^2}$; and the effective impedances of the perpendicular polarized wave are $Z_{m0} = \sqrt{u_0/\varepsilon_0}\sec\theta_m$, $Z_{mL_m+1} = \sqrt{u_0/\varepsilon_{mL_m+1}}\sec\theta_{mL_m+1}$, $\sec\theta_{mL_m+1} = 1/\sqrt{1 - \left(\sqrt{\frac{\varepsilon_0}{\varepsilon_{mL_m+1}}}\sin\theta_m\right)^2}$.

$$R_m\left(n_{e,mi}, v_{mi}, f, \theta_m, L_m\right) = \begin{cases} \dfrac{(A_m + B_m/Z_{mL_m+1}) - Z_{m0}(C_m + D_m/Z_{mL_m+1})}{(A_m + B_m/Z_{mL_m+1}) + Z_{m0}(C_m + D_m/Z_{mL_m+1})}, & L_m \neq N_m \\ \dfrac{B_m - D_m Z_{m0}}{B_m + D_m Z_{m0}}, & L_m = N_m \end{cases} \tag{23}$$

$$E_m\left(n_{e,mi}, v_{mi}, f, \theta_m, L_m, \varphi, \gamma\right) = \Gamma_m R_m\left(n_{e,mi}, v_{mi}, f, \theta_m, L_m\right) e^{-j4\pi(f + f_{Dm}(L_m))r_m(\varphi,\gamma)/c} \tag{25}$$

$$\mathrm{r}_m(\varphi, \gamma) = \begin{cases} x_m \cos\gamma \cos\varphi + y_m \cos\gamma \sin\varphi + z_m \sin\gamma - (\sum_{i=L_m+1}^{N_m} d_{mi}) \cos\theta_m, & L_m \neq N_m \\ x_m \cos\gamma \cos\varphi + y_m \cos\gamma \sin\varphi + z_m \sin\gamma, & L_m = N_m \end{cases} \tag{26}$$

$$E\left(n_{e,mi}, v_{mi}, f, \theta_m, L_m, \varphi, \gamma\right) = \sum_{m=1}^{M} E_m\left(n_{e,mi}, v_{mi}, f, \theta_m, L_m, \varphi, \gamma\right) \tag{27}$$

And Doppler frequency are rewritten as the following form:

$$f_{Dm}(L_m) = \begin{cases} -2\dfrac{f}{c} V_{f,mL_m} \sin\theta_m, & L_m \neq N_m \\ -2\dfrac{f}{c} V_0 \cos\gamma \cos\varphi, & L_m = N_m, \end{cases} \tag{24}$$

where, $f = \omega/2\pi$ is the frequency of the incident wave (Hz), c is velocity of light.

Step 5: Based on (1), the radar echo signal of the mth scattering center can be described as (25), where $f + f_{Dm}(L_m) = f_R$. Based on (2) and incident depth L_m, $r_m(\varphi, \gamma)$ can be rewritten as (26). Finally, the radar echo signal of the reentry object covered with plasma sheath can be expressed as (27). Formula (25)–(27) are shown at the top of this page.

The important steps will be explained in detail below.

A. INCIDENCE ANGLE OF THE ELECTROMAGNETIC WAVE

The incident angle of the electromagnetic wave is the angle between the incident plane of the electromagnetic wave and the normal of the layered model. The incident angle is related to the elevation angle, flying attitude, and structure of the target. This paper takes a blunt cone as an example to illustrate the calculation of the incident angle of the electromagnetic wave, as shown in Figure 6.

After the projection angles of the incident angle of the electromagnetic wave on the YZ plane and XY plane are obtained, the incident angle of the electromagnetic wave can be obtained by (14).

B. DOPPLER FREQUENCY

Considering that the non-mirror trajectory in Fig. 1 has an obvious signal broadening phenomenon, the present paper assumes that the Doppler frequency of the plasma sheath is related to the position of the reflection of the electromagnetic wave. The signal broadening is caused by the difference in the Doppler frequency shift of the signal component.

For radar, the Doppler frequency of the target is defined as

$$f_D = -f\frac{2V}{c}, \tag{28}$$

where V is the target radial velocity along the line of sight. For rigid objects, all scattering centers have the same Doppler frequency when only translational motion exists. Velocity is defined as being positive when the target is far from the radar system. The plasma sheath is different from the traditional rigid-body target, and its velocity is not unique.

In the plasma sheath, plasma flows backward radially from the stagnation point. Compared with the inner airflow, the outer airflow diffuses outward at varying degrees under the influence of the flight speed, which results in a different direction of airflow velocity in the plasma sheath in three-dimensional space. The proposed model simplifies the direction of the airflow velocity and assumes that the direction of the airflow velocity at the same scattering center is the same. In addition, because the incident depth of the electromagnetic wave is affected by both the plasma frequency and electromagnetic wave frequency, it indirectly affects the extraction of the target velocity. The velocity of airflow increases toward the reentry surface. It is therefore necessary to determine the type of reflection medium according to the incident depth, then extract the corresponding type of velocity, and finally obtain the Doppler frequency. It is worth noting that the stagnation point of the plasma sheath is located at the front end of the reentry object, and the speed and direction of movement of the stagnation point are thus the same as those of the reentry object. So the numerical value and direction of airflow velocity in the layered model of stagnation point are the same as that of the reentry object.

C. RADAR ECHO

Combining (1) and (28), radar echo signals of targets not affected by plasma sheath can be written as:

$$E(\varphi, \gamma, f) = \sum_{m=1}^{M} \Gamma_m e^{-j4\pi(f + f_D)r_m(\varphi,\gamma)/c}, \tag{29}$$

where, $f + f_D = f_R$. Let $e^{-j4\pi r_m(\varphi,\gamma)/c} = e^{-j\Theta}$, formula (29) can be rewritten as:

$$E(f) = \sum_{m=1}^{M} \Gamma_m e^{-jf\Theta} e^{-jf_D\Theta}. \tag{30}$$

As shown in formula (25, 26, 27), the radar echo signal under the influence of plasma sheath is as (31). Ibid., radar echo signals can be rewritten as (32). Formula (31) and (32) are shown at the bottom of the next page.

Formulas (30) and (32) represent radar echo signals of reentry objects without plasma sheath and covered with plasma sheath, respectively. It can be seen that component $e^{-jf_D\Theta}$ in formula (30) becomes components $R_m\left(n_{e,mi}, v_{mi}, f, \theta_m, L_m\right)$ and $e^{-jf_{Dm}\Theta}$ of formula (32) under the influence of plasma sheath.

Without considering the plasma sheath, the velocity of scattering centers is the same, so the $e^{-jf_D\Theta}$ of scattering centers is the same; and under the influence of plasma sheath, the velocity of scattering centers is independent and different from each other, so the echo signal $e^{-jf_{Dm}\Theta}$ of scattering centers is also independent from each other (the numerical value is determined by the incident depth, incident angle and velocity of the flow field). And the reflection coefficient $R_m\left(n_{e,mi}, v_{mi}, f, \theta_m, L_m\right)$ of scattering centers will modulate the amplitude and phase of radar echo signal, which will cause amplitude attenuation and phase shift intuitively.

IV. EXAMPLE

The present paper uses the computational-fluid-dynamics flow-field simulation data of RAM-C for the reentry vehicle [26]. The target flying state is set as forward-to-radar level flight with an elevation angle of 30 degrees, a flying altitude of 30 km, and a flying speed of 25 Ma. To reduce the computational complexity, only the lower half of the plasma sheath is modeled in this paper.

Simulation results of radar detection pulse compression are obtained by setting the radar type as X-band broadband radar, carrier center frequency $f_z = 9GHz$, bandwidth $B = 1GHz$ pulse width $\tau = 400\mu s$, and sampling frequency $f_s = 5GHz$ and using (17).

Figure 8 shows two strong reflection signals. According to calculation results of the plasma frequency, an electromagnetic wave cannot penetrate the plasma sheath and all target reflection signals are reflected in the plasma. It is noteworthy that the plasma wake is not modeled in this paper.

According to the order from head to tail and from left to right, the incident depth, radial velocity, and reflection coefficient of 51 scattering centers are listed in Table 1.

Table 1 (a) gives the incident depth of the electromagnetic wave. The incident depth is shallowest at the stagnation point of the plasma sheath and increases as the incident depth approaches the tail. Table 1 (b) gives the radial velocity of each scattering center in a unit of Ma. The radial velocity is largest at the stagnation point. The closer the remaining scattering centers are to the tail, the greater the radial velocity is, and the closer the radial velocity is to both sides. Table 1 (c) gives the normalized reflection coefficients of the scattering centers. The reflection coefficient is largest at the stagnation point and decreases as the scattering center approaches the tail.

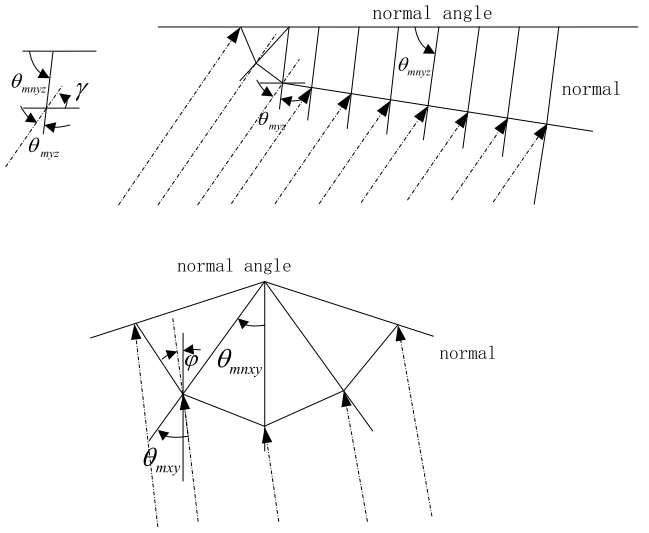

FIGURE 6. Schematic diagram for calculating the incident angle of the electromagnetic wave. $\theta_{myz} = \theta_{mnyz} - \gamma$, $\theta_{mxy} = \theta_{mnxy} + \varphi$, the central symmetric axis of the blunt cone, is parallel to the x-axis. θ_{myz} and θ_{mnyz} are respectively projections of the incident angle and normal wrestling angle of the electromagnetic wave on the YZ plane. θ_{mxy} and θ_{mnxy} are respectively the projections of the incident angle and normal angle of the electromagnetic wave on the XY plane.

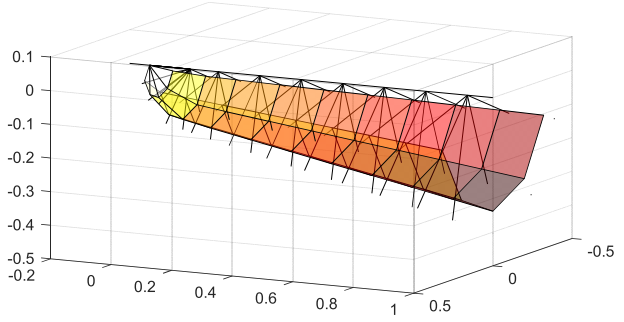

FIGURE 7. Distribution of scattering centers of a blunt cone. The blunt cone has a length of 1.295 m, radius of 0.159 m, and semi-cone angle of 9°. With the stagnation point as the vertex, the cone is divided into 11 rows and 5 rows from beginning to end, generating a total of 51 scattering centers. The plasma parameters in the layered model are the same as those of the scattering centers of the same row.

An analysis of the radial velocity and reflection coefficients of 51 scattering centers shows that the left peak is the reflection signal of the stagnation point and the right peak is the reflection signal of other scattering centers of the spherical head. Because of the radial velocity, the scattering centers, which are originally about 0.15 m apart, are about 4 m apart in the pulse compression results. The reflection

$$E\left(n_{e,mi}, v_{mi}, f, \theta_m, L_m, \varphi, \gamma\right) = \sum_{m=1}^{M} \Gamma_m R_m(n_{e,mi}, v_{mi}, f, \theta_m, L_m) e^{-j4\pi(f+f_{Dm}(L_m))r_m(\varphi,\gamma)/c} \tag{31}$$

$$E(n_{e,mi}, v_{mi}, f, \theta_m, L_m) = \sum_{m=1}^{M} \Gamma_m e^{-jf\Theta} \cdot R_m\left(n_{e,mi}, v_{mi}, f, \theta_m, L_m\right) e^{-jf_{Dm}\Theta} \tag{32}$$

TABLE 1. (a) Incident depth. (b) Radial velocity. (c) Reflection coefficient.

(A) INCIDENT DEPTH

	1	2	3	4	5	6	7	8	9	10	11
Incident depth	3	4	3	6	8	14	23	23	25	26	28
Total layer number	17	27	23	35	41	46	55	48	47	45	45
Penetration ratio（%）	17.6	14.8	13	17.1	19.5	30.4	41.8	47.9	53.2	57.8	62.2

(B) RADIAL VELOCITY

	1	2	3	4	5	6	7	8	9	10	11
1	-	2.06	5.96	15.48	17.70	17.63	17.83	18.08	18.29	18.40	18.68
2	-	1.28	4.73	13.26	15.16	15.10	15.27	15.48	15.66	15.76	16.00
3	21.58	0.23	4.18	12.56	14.37	14.31	14.48	14.67	14.85	14.94	15.16
4	-	1.28	4.73	13.26	15.16	15.10	15.27	15.48	15.66	15.76	16.00
5	-	2.06	5.96	15.48	17.70	17.63	17.83	18.08	18.29	18.40	18.68

(C) REFLECTION COEFFICIENT

	1	2	3	4	5	6	7	8	9	10	11
1	-	149.1	66.38	13.97	5.945	6.584	3.631	1.544	2.102	3.113	2.753
2	-	80.47	72.15	9.745	4.921	5.457	2.108	1.387	2.763	2.714	2.227
3	254	107.0	17.02	17.04	1.663	6.546	2.044	2.948	1.149	1	3.255
4	-	80.47	72.15	9.745	4.921	5.457	2.108	1.387	2.763	2.714	2.227
5	-	149.1	66.38	13.97	5.945	6.584	3.631	1.544	2.102	3.113	2.753

The unit of radial velocity is Mach. Reflection coefficient is the result of normalization

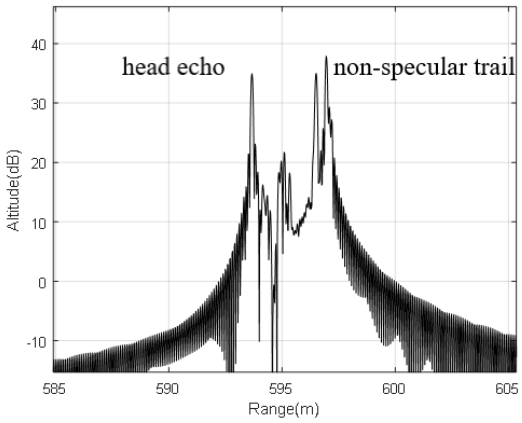

FIGURE 8. Simulation results of radar detection pulse compression. The reflected signal on the left can be regarded as head echo, while the two signal peaks on the right can be regarded as non-mirror trajectories.

signal of the cone body is located between the two peaks and is relatively weak.

Two reflected signals can be clearly distinguished from the simulation results of pulse compression, which shows to some extent that the plasma wake is not the cause of non-specular echoes. We believe that the non-mirror reflection signal is produced by the non-uniform plasma distribution and the gradient airflow velocity distribution of the plasma sheath. The main component of the non-specular echoes is produced by the superficial reflection of the plasma sheath. Because the velocity of stagnation point is much larger than that of shallow airflow at other scattering centers, there is a certain separation of the two strong reflection signals, and the width of the separation is not fixed but changes with the electromagnetic wave frequency, plasma parameters, and flight speed.

V. CONCLUSION

The present paper proposed a method with which to model the radar scattering center of a reentry object covered by a plasma sheath. Because of the combination of the scattering center model and non-uniform plasma layered model, the simulation of a radar echo is more realistic, which satisfies the detection characteristics of broadband radar and takes into account the non-uniform distribution characteristics of the plasma sheath. In particular, each scattering center can be used to calculate the incident angle, incident depth, radial velocity, and reflection coefficient independently, which is the key to building the scattering center model of a reentry object covered by a plasma sheath. The only deviation from the actual situation is that all interfaces of the layered model of the non-uniform plasma are parallel. However, from the point of view of convenient calculation, we do not recommend making more adjustments because an increase in the numbers of layers and incident angles will increase the calculation cost. It will undoubtedly become difficult to simulate the radar echo of a complex reentry object covered by a plasma sheath. Our experience has shown that the reflection coefficient adds most to the computational expense. If the flight process of the target is fixed, it is suggested that the calculation results of the reflection coefficient be saved as a database.

The proposed modeling method effectively reflects the plasma distribution and electromagnetic-wave propagation characteristics of the plasma sheath. Although the simulation is only a steady-state simulation of a single pulse at present, it provides a basis for the radar echo simulation of a time-varying plasma sheath. The calculation cost is large because of the complexity of the model. The present paper generated only one reflection signal for each scattering center and analyzed only the main components of the head echo and non-specular echo (i.e., the reflection signal at the stagnation point

and superficial surface of the plasma sheath). To some extent, it is shown that the non-specular echo is not generated by the plasma wake, but by the multi-layer plasma in the part penetrated by the electromagnetic wave under the combined effect of the non-uniform plasma distribution and the gradient airflow velocity distribution. This provides a new idea for radar detection and the signal processing of reentry objects covered by a plasma sheath. At the same time, establishing a good scattering model of a reentry object covered by a plasma sheath can generate a real-time target signal, which greatly reduces the demand for electromagnetic simulation software code and measurement data and provides convenience for subsequent related research.

ACKNOWLEDGMENT

The authors would like to thank Weifang Chen, Prof, from College of Aeronautics and Astronautics, Zhejiang University, Hangzhou, China, for giving flow-field simulation data of RAM-C.

REFERENCES

[1] D. M. Dix, "Typical values of plasma parameters around a conical re-entry vehicle," Aerosp. Corp., El Segundo, CA, USA, Sci. Rep. AD295429, Nov. 1962.

[2] S. Close, M. Oppenheim, S. Hunt, and L. Dyrud, "Scattering characteristics of high-resolution meteor head echoes detected at multiple frequencies," *J. Geophys. Res. Space Phys.*, vol. 107, no. A10, pp. SIA 9-1–SIA 9-12, 2002.

[3] L. Dyrud, D. Wilson, S. Boerve, J. Trulsen, H. Pecseli, S. Close, C. Chen, and Y. Lee, "Plasma and electromagnetic simulations of meteor head echo radar reflections," *Adv. Meteoroid Meteor Sci.*, vol. 102, nos. 1–4, pp. 383–394, 2008.

[4] B. Bai, Y. Liu, L. Song, X. Li, Y. Ding, and X. Zhang, "Passive radar jamming: A novel method using time-varying plasma," *IEEE Access*, vol. 7, pp. 120082–120088, 2019.

[5] B. X. Jiang, X. Yang, P. Ma, B. Chen, J. Tian, A. Shi, and P. Tang, "Contactless measurement of hypervelocity projectile wake velocity distribution," *IEEE Access*, vol. 7, pp. 28968–28972, 2019.

[6] M. Laroussi and J. R. Roth, "Numerical calculation of the reflection, absorption, and transmission of microwaves by a nonuniform plasma slab," *IEEE Trans. Plasma Sci.*, vol. 21, no. 4, pp. 366–372, Aug. 1993.

[7] V. R. Goteti and D. K. Kalluri, "Wave propagation in a switched-on time-varying plasma medium," *IEEE Trans. Plasma Sci.*, vol. 17, no. 5, pp. 828–833, Oct. 1989.

[8] D. K. Kalluri, V. R. Goteti, and A. M. Sessler, "WKB solution for wave propagation in a time-varying magnetoplasma medium: Longitudinal propagation," *IEEE Trans. Plasma Sci.*, vol. 21, no. 1, pp. 70–76, Feb. 1993.

[9] J. H. Lee and D. K. Kalluri, "Three-dimensional FDTD simulation of electromagnetic wave transformation in a dynamic inhomogeneous magnetized plasma," *IEEE Trans. Antennas Propag.*, vol. 47, no. 7, pp. 1146–1151, Jul. 1999.

[10] J.-F. Liu, X.-L. Xi, G.- B. Wan, and L.-L. Wang, "Simulation of electromagnetic wave propagation through plasma sheath using the moving-window finite-difference time-domain method," *IEEE Trans. Plasma Sci.*, vol. 39, no. 3, pp. 852–855, Mar. 2011.

[11] S.-H. Liu and L.-X. Guo, "Analyzing the electromagnetic scattering characteristics for 3-D inhomogeneous plasma sheath based on PO method," *IEEE Trans. Plasma Sci.*, vol. 44, no. 11, pp. 2838–2843, Nov. 2006.

[12] S. Liu and S.-Y. Zhong, "Analysis of backscattering RCS of targets coated with parabolic distribution and time-varying plasma media," *Optik*, vol. 124, no. 24, pp. 6850–6852, 2013.

[13] H.-C. Deng, X. Wei, and H.-C. Yin, "EM scattering analysis of complex target coated with plasma by conformal SO-FDTD method," in *Proc. IEEE Int. Conf. Green Comput. Commun. IEEE Internet Things IEEE Cyber, Phys. Social Comput.*, Beijing, China, vol. 273, Aug. 2013, pp. 1538–1541.

[14] G. Wang, L. Yuan, T. Wang, N. Fang, J. Miao, and B. Wang, "RCS calculation of complex targets shielded with plasma based on visual GRECO method," in *Proc. 3rd IEEE Int. Symp. Microw., Antenna, Propag. EMC Technol. Wireless Commun.*, Oct. 2009, pp. 950–953.

[15] X.-Y. Chen, K.-X. Li, Y.-Y. Liu, Y.-G. Zhou, X.-P. Li, and Y.-M. Liu, "Study of the influence of time-varying plasma sheath on radar echo signal," *IEEE Trans. Plasma Sci.*, vol. 45, no. 12, pp. 3166–3176, Dec. 2017.

[16] C. R. Luo, C. L. Ding, and L. B. Duan, *12th Five-Year Plan Textbooks: Electrodynamics*. Beijing, China: Publishing House of Electronics Industry, 2016, pp. 150–176.

[17] C. Q. Cao, *Basic Series of Modern Physics Classical Electrodynamics*. Beijing, China: Science Press, 2009, pp. 167–180.

[18] S. H. Guo, *12th Five-Year National Plan Textbooks: Electrodynamics*. Beijing, China: Higher Education Press, 2018, pp. 146–150.

[19] J. Xu, B. Bai, C. Dong, and G. Zhao, "A novel passive jamming method against ISAR based on resonance absorption effect of metamaterials," *IEEE Access*, vol. 6, pp. 18142–18148, 2018.

[20] Z. L. Wang, Y. Wang, L. Zhu, W. Ma, J. Shan, and F. Liu, "Experimental study of influence on microwave plasma ignition combustion performance of pulse microwave signals," *IEEE Access*, vol. 7, pp. 23951–23958, 2019.

[21] Z. Jianxiong, S. Zhiguang, C. Xiao, and F. Qiang, "Automatic target recognition of SAR images based on global scattering center model," *IEEE Trans. Geosci. Remote Sens.*, vol. 49, no. 10, pp. 3713–3729, Oct. 2011.

[22] Y. Akyildiz and R. L. Moses, "Scattering center model for SAR imagery," *Proc. SPIE*, vol. 3869, pp. 76–85, Dec. 1999.

[23] H.-P. Ip and Y. Rahmat-Samii, "Analysis and characterization of multilayered reflector antennas: Rain/snow accumulation and deployable membrane," *IEEE Trans. Antennas Propag.*, vol. 46, no. 11, pp. 1593–1605, Nov. 1998.

[24] H. Meng, W. Dou, T. Chen, and K. Yin, "Analysis of radome using aperture integration-surface integration method with modified transmission coefficient," *J. Infr. Millim. THz Waves*, vol. 30, pp. 199–210, Feb. 2009.

[25] B. Bai, X. Li, X. Jin, and Y. Liu, "Reflections of electromagnetic waves obliquely incident on a multilayer stealth structure with plasma and radar absorbing material," *IEEE Trans. Plasma Sci.*, vol. 43, no. 8, pp. 2588–2597, Aug. 2015.

[26] W. F. Chen and W. W. Zhao, *Rarefied Gas Dynamic Moment Method and Numerical Simulation*. Beijing, China: Science Press, 2017, pp. 252–258.

XI ZHANG was born in 1990. She received the B.S. and M.S. degrees in information and communication engineering from Xidian University, China, in 2015, where she is currently pursuing the Ph.D. degree.

From 2012 to 2015, she worked in radar signal processing experiments on meter-wave radar altimetry. Since 2015, she has been with the School of Aerospace Science and Technology, Xidian University, where she has been involved in radar signal processing theory.

YANMING LIU was born in 1966. He received the Ph.D. degree from Xidian University, China, in 2003, where he is currently a Professor with the School of Aerospace Science and Technology. His research interests include TT&C communication of the near-space aircraft, space-air-ground information networks, and space physics characteristics.

BOWEN BAI was born in Weinan, Shaanxi, China, in 1986. He received the B.S. and Ph.D. degrees from Xidian University, Xi'an, China, in 2010 and 2015, respectively. His current research interest includes the interaction of electromagnetic waves with the plasma and radiation of antenna covered by the plasma.

XIAOPING LI was born in Shaanxi, China, in 1961. She received the B.S., M.S., and Ph.D. degrees from Xidian University, Xi'an, China, in 1982, 1988, and 2004, respectively.

She is currently a Full Professor with the School of Aerospace Science and Technology, Xidian University. Her current research interests include the near-space vehicle's telemetry tracking, and command and communication technology.

FANGFANG SHEN received the B.S., M.S., and Ph.D. degrees in telecommunications engineering from Xidian University, Xi'an, China, in 2006, 2009, and 2015, respectively, where she is currently a Teacher with the School of Aerospace Science and Technology. Her research interests include high-resolution radar imaging and DOA estimation.

XU-YANG CHEN was born in Chengde, China, in 1980. He received the B.S., M.S., and Ph.D. degrees in electronic engineering from Xidian University, Xi'an, China, in 2005, 2008, and 2011, respectively. He joined the CAST-Xi'an Institute of Space Radio Technology, Xi'an, as an Engineer, in 2011, where he is involved in radar detection and space navigation. He is currently a Teacher with the School of Aerospace Science and Technology, Xidian University. His current research interest includes the radar detection of reentry vehicles covered by plasma sheath.

LIANG ZHAO was born in Inner Mongolia Autonomous Region. He is currently a Senior Engineer of Professor. His research interest includes spacecraft TT&C and communication systems.